Electronic Supplementary Material to: The Relationship between Model Biases in East Asian Summer Monsoon Rainfall and Land Evaporation

Ruth GEEN[1,2], Marianne PIETSCHNIG[2], Shubhi AGRAWAL[3,2], Dipanjan DEY[4,2], F. Hugo LAMBERT[2], and Geoffrey K. VALLIS[2]

[1]*School of Geography, Earth and Environmental Sciences, University of Birmingham, Birmingham B*15 2*TT, UK*

[2]*Department of Mathematics and Statistics, University of Exeter, Exeter EX*4 4*QJ, UK*

[3]*Department of Earth and Environmental Sciences, Indian Institute of Science Education and Research, Bhopal* 462 066, *India*

[4]*School of Ocean and Earth Science, University of Southampton, Southampton SO*17 1*BJ, UK*

ESM to: Geen, R., M. Pietschnig, S. Agrawal, D. Dey, F. H. Lambert, and G. K. Vallis., 2023: The relationship between model biases in East Asian Summer Monsoon rainfall and land evaporation. *Adv. Atmos. Sci.*, **40**(11), 2029–2042, https://doi.org/10.1007/s00376-023-2297-1.

1. Bucket model

The model uses a bulk formula to calculate the surface latent heat flux:

$$E = \beta \rho_a C |v_a| (q_a - q_s) \ ,$$

where E is evaporation, ρ_a, $|v_a|$ and q_a are the density, horizontal wind speed and specific humidity at the lowest model level, C is the drag coefficient, and q_s is the saturation specific humidity at the surface temperature (cf. Eq. 11, Frierson et al., 2006). Over ocean, the evaporative resistance parameter β =1. Land evaporation is differentiated from that over ocean by varying β. In the *dry-land* simulation presented here β =0, while in the *ocean-land* simulation β =1.

For the *bucket* simulation, a simple bucket hydrology is used to describe evapotranspiration (cf. Manabe, 1969; Pietschnig et al., 2019). The bucket can contain a depth of water, W, up to a field capacity, $W_{\rm FC}$, which is set to 1 m in the simulation presented here. The bucket is initialized as full. During the simulation, the bucket's water depth is modified by precipitation, P, and evaporation so that:

$$\frac{{\rm d}W}{{\rm d}t} = P - E \text{ if } W < W_{\rm FC} \text{ or } P < E \ ,$$

$$\frac{{\rm d}W}{{\rm d}t} = 0 \text{ if } W = W_{\rm FC} \text{ and } P > E \ ,$$

The bucket depth then modifies β in the bulk formula as:

$$\beta = 1 \text{ if } W \geqslant 0.75 W_{\rm FC} \ ,$$

$$\beta = \frac{W}{0.75 W_{\rm FC}} \text{ if } W < 0.75 W_{\rm FC} \ .$$

2. CMIP6 simulation data used

Table S1 summarizes the CMIP6 models, simulations and variants used in this study. 40 models were selected based on availability of data for: precipitation, surface soil moisture, surface temperature and pressure, top of atmosphere and surface radiative and turbulent energy fluxes, near surface air temperature, horizontal windspeeds, temperature, specific humidity

*The online version of this article can be found at https://doi.org/10.1007/s00376-023-2297-1.

Table S1. Summary of CMIP6 simulations used in this study.

Model name	amip	*historical*	*land-hist*
ACCESS-CM2	r1i1p1f1	r1i1p1f1	
ACCESS-ESM1-5	r1i1p1f1	r1i1p1f1	
BCC-CSM2-MR	r1i1p1f1	r1i1p1f1	
BCC-ESM1	r1i1p1f1	r1i1p1f1	
CAMS-CSM1-0	r1i1p1f1	r1i1p1f1	
CAS-ESM2-0	r1i1p1f1	r1i1p1f1	
CESM2	r1i1p1f1	r1i1p1f1	r1i1p1f1
CESM2-WACCM	r1i1p1f1	r1i1p1f1	
CMCC-CM2-HR4	r1i1p1f1	r1i1p1f1	
CMCC-CM2-SR5	r1i1p1f1	r1i1p1f1	r1i1p1f1
CNRM-CM6-1	r1i1p1f2	r1i1p1f2	r1i1p1f2
CNRM-CM6-1-HR	r1i1p1f2	r1i1p1f2	
CNRM-ESM2-1	r1i1p1f2	r1i1p1f2	r1i1p1f2
CanESM5	r1i1p1f1	r1i1p1f1	
E3SM-1-0	r1i1p1f1	r1i1p1f1	
EC-Earth3	r1i1p1f1	r1i1p1f1	
EC-Earth3-CC	r1i1p1f1	r1i1p1f1	
EC-Earth3-Veg	r1i1p1f1	r1i1p1f1	r1i1p1f1
FGOALS-f3-L	r1i1p1f1	r1i1p1f1	
FGOALS-g3	r1i1p1f1	r1i1p1f1	r1i1p1f1
GFDL-CM4	r1i1p1f1	r1i1p1f1	
GISS-E2-1-G	r1i1p1f1	r1i1p1f1	
HadGEM3-GC31-LL	r1i1p1f3	r1i1p1f3	r1i1p1f3
HadGEM3-GC31-MM	r1i1p1f3	r1i1p1f3	
INM-CM4-8	r1i1p1f1	r1i1p1f1	
INM-CM5-0	r1i1p1f1	r1i1p1f1	
IPSL-CM6A-LR	r1i1p1f1	r1i1p1f1	r1i1p1f1
KACE-1-0-G	r1i1p1f1	r1i1p1f1	
MIROC6	r1i1p1f1	r1i1p1f1	r1i1p1f1
MIROC-ES2L	r1i1p1f2	r1i1p1f2	
MPI-ESM1-2-HAM	r1i1p1f1	r1i1p1f1	
MPI-ESM1-2-HR	r1i1p1f1	r1i1p1f1	
MPI-ESM1-2-LR	r1i1p1f1	r1i1p1f1	r1i1p1f1
MRI-ESM2-0	r1i1p1f1	r1i1p1f1	
NorCPM1	r1i1p1f1	r1i1p1f1	
NorESM2-LM	r1i1p1f1	r1i1p1f1	
SAM0-UNICON	r1i1p1f1	r1i1p1f1	
TaiESM1	r1i1p1f1	r1i1p1f1	
UKESM1-0-LL	r1i1p1f4	r1i1p1f2	r1i1p1f2
UKESM1-1-LL	r1i1p1f2	r1i1p1f2	

and geopotential height (variables hfls, hfss, hus, mrsos, pr, ps, rlds, rlus, rlut, rsds, rsdt, rsus, rsut, ta, tas, ts, ua, va, zg).

Data is used for 11 *land-hist* simulations in which the land model matches available AMIP and *historical* simulation data. A *land-hist* simulation was not explicitly performed for CMCC-CM2-SR5. However, CMCC-CM2-SR5 uses the same land model as CMCC-ESM2 for which *land-hist* data was available. The CMCC-ESM2 *land-hist* data is therefore used here for comparison with the CMCC-CM2-SR5 AMIP and *historical* simulations.

3. Supplementary Figures

Figures S1–S11 are provided at the end of this document to support the main text.

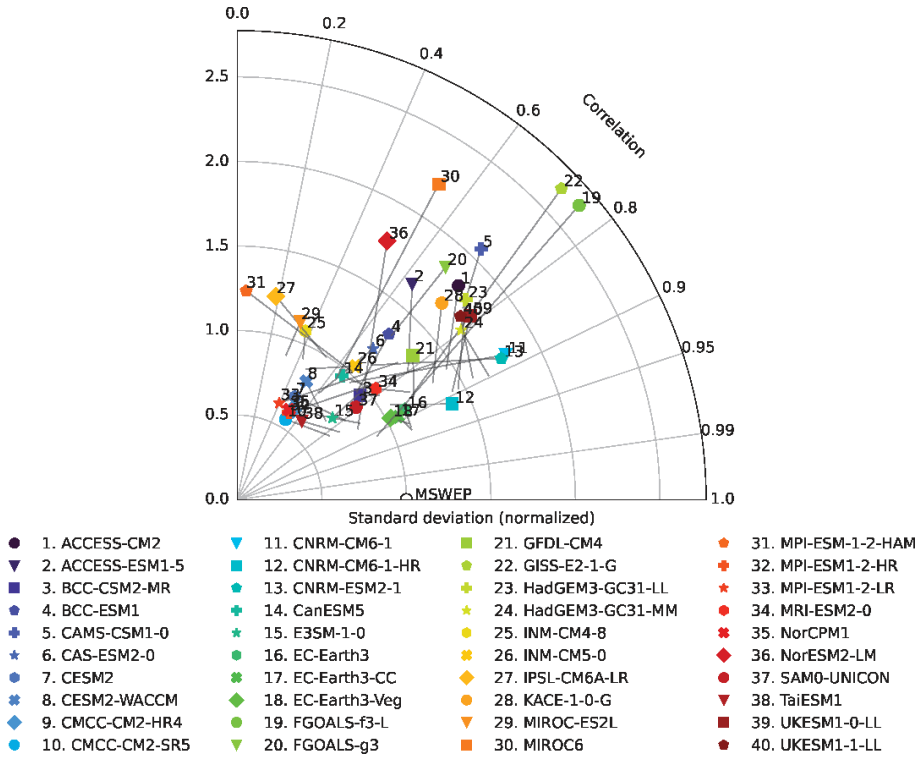

Fig. S1. Taylor diagram comparing model skill at simulating climatological East Asian summer monsoon precipitation (JJA, 1980–2014; 110°–140°E, 0°–45°N) in the AMIP and coupled-ocean experiments. For each model, the AMIP simulation values are indicated by symbols. Lines beginning from each symbol terminate at the pattern correlation and normalized standard deviation value for the respective coupled-ocean simulation. Models are compared against the MSWEP 1980–2014 climatology (Beck et al., 2019), which is marked by the circle on the horizontal axis. The coupled-ocean simulations generally show higher skill in representing observed EASM precipitation than is achieved by the atmosphere-only models, with the least skillful atmosphere-only models improved the most by coupling.

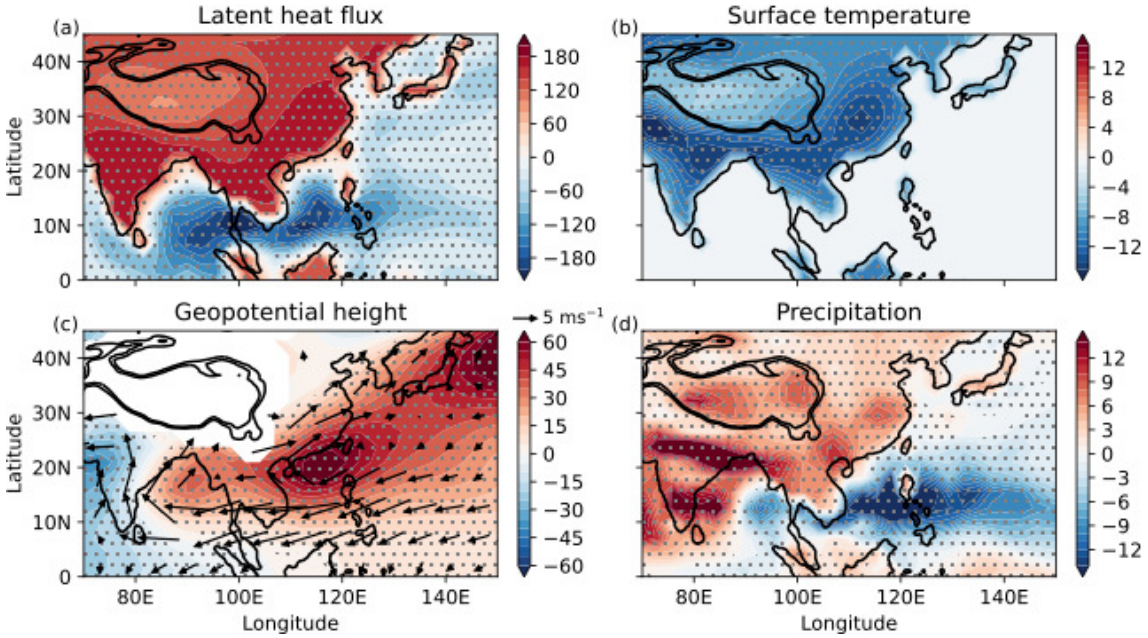

Fig. S2. As Fig. 2 in the main text, but showing differences between the *ocean-land* and *dry-land* simulations.

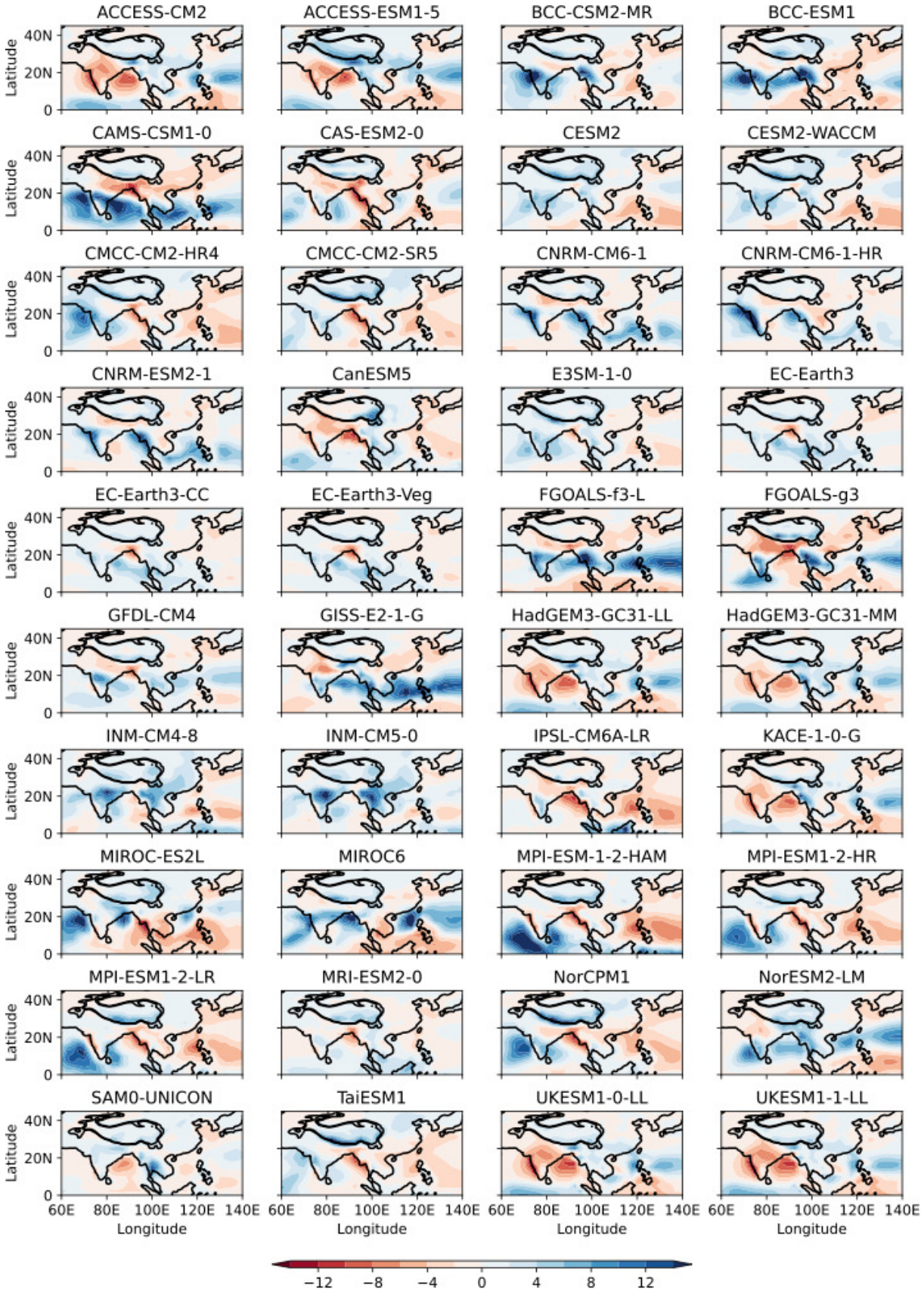

Fig. S3. Difference in JJA climatological precipitation (mm d^{-1}) between the AMIP simulations used in this study and MSWEP.

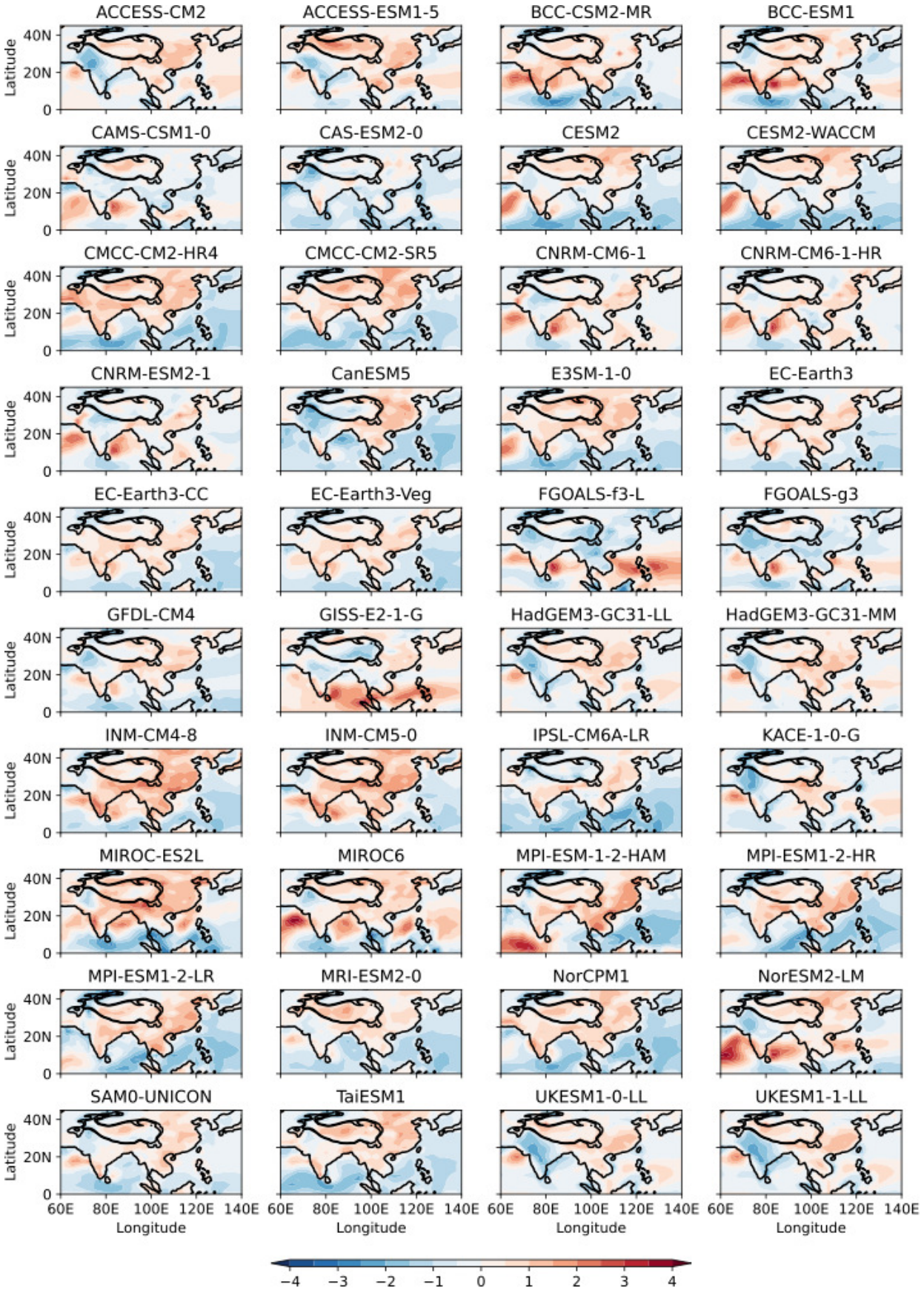

Fig. S4. Difference in JJA climatological evaporation (mm d^{-1}) between the AMIP simulations used in this study and JRA-55.

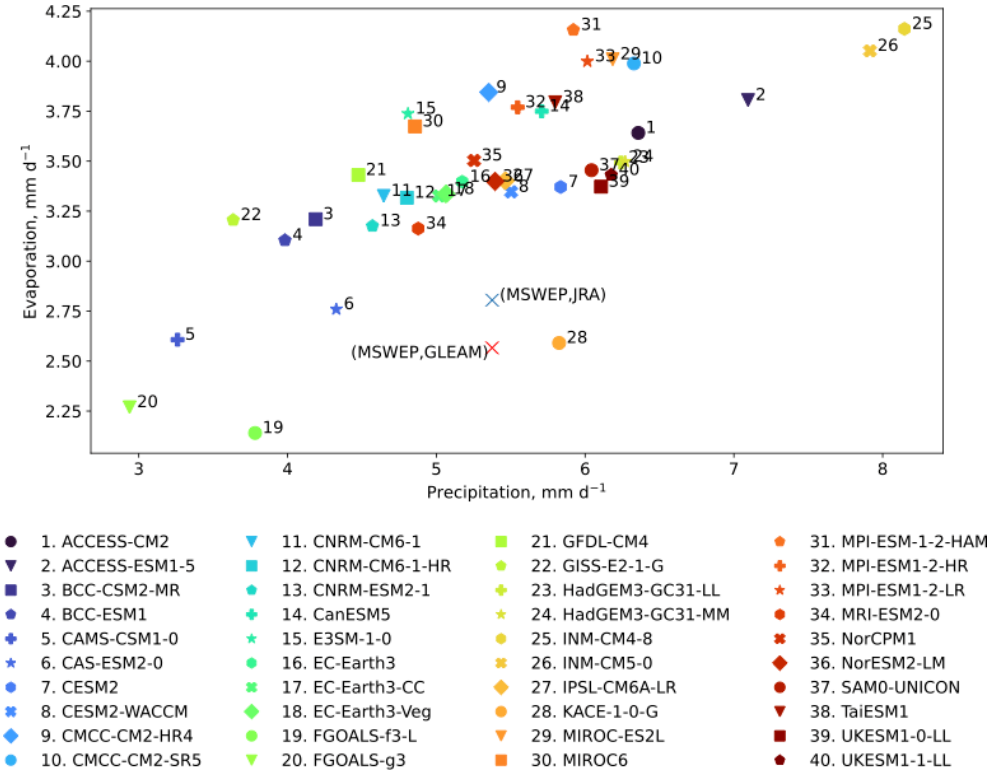

Fig. S5. Scatter plot showing the JJA climatological-mean values of precipitation and evaporation over land in the box 110°–120°E, 20°–40°N for each AMIP simulation used. Observed values are indicated by blue (MSWEP & JRA-55) and red (MSWEP & GLEAM) crosses. The multi-model mean values are 5.37 mm d^{-1} for precipitation with standard deviation 1.01 mm d^{-1}, and 3.43 mm d^{-1} for evaporation with standard deviation 0.46 mm d^{-1}.

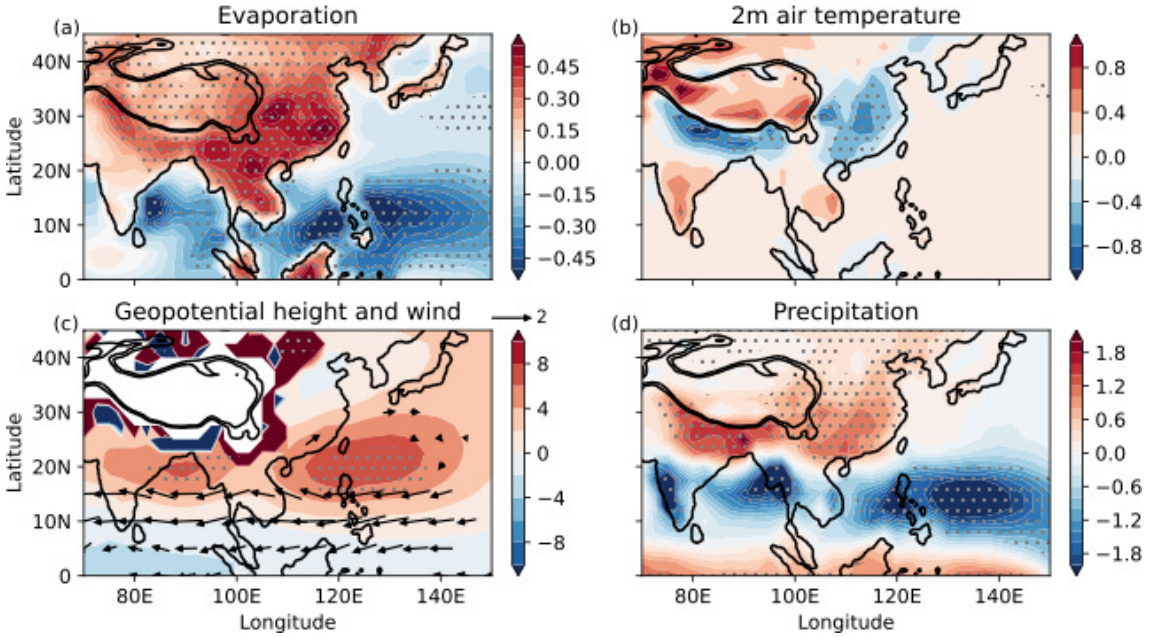

Fig. S6. As Fig. 3 in the main text, but showing the regression against normalized global-mean land evaporation.

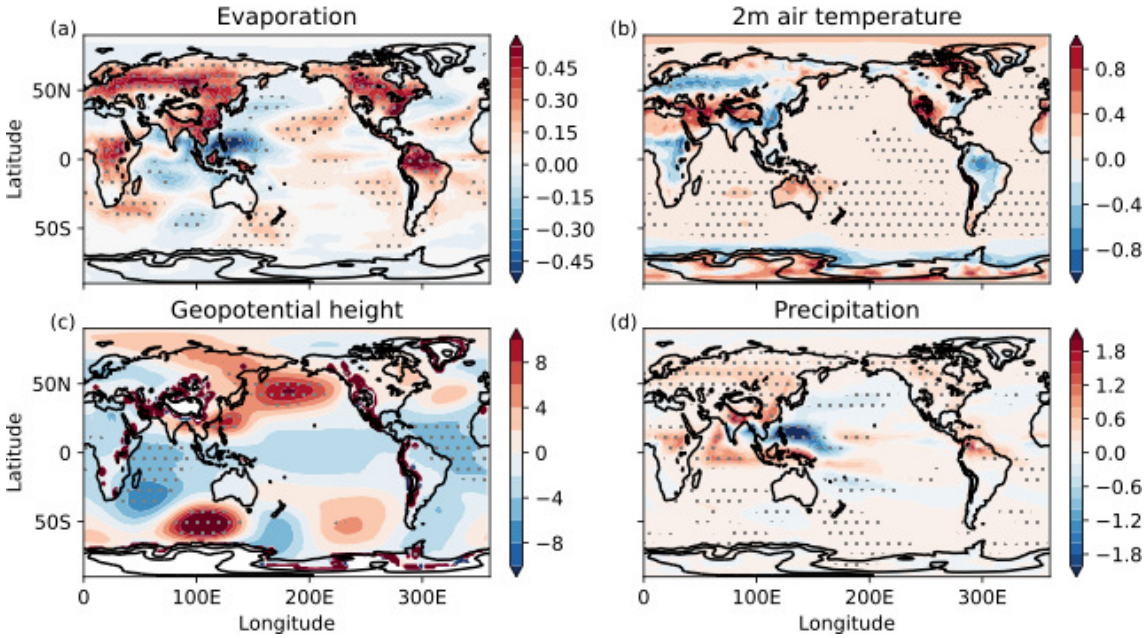

Fig. S7. As Fig. 3 in the main text, but showing the global domain.

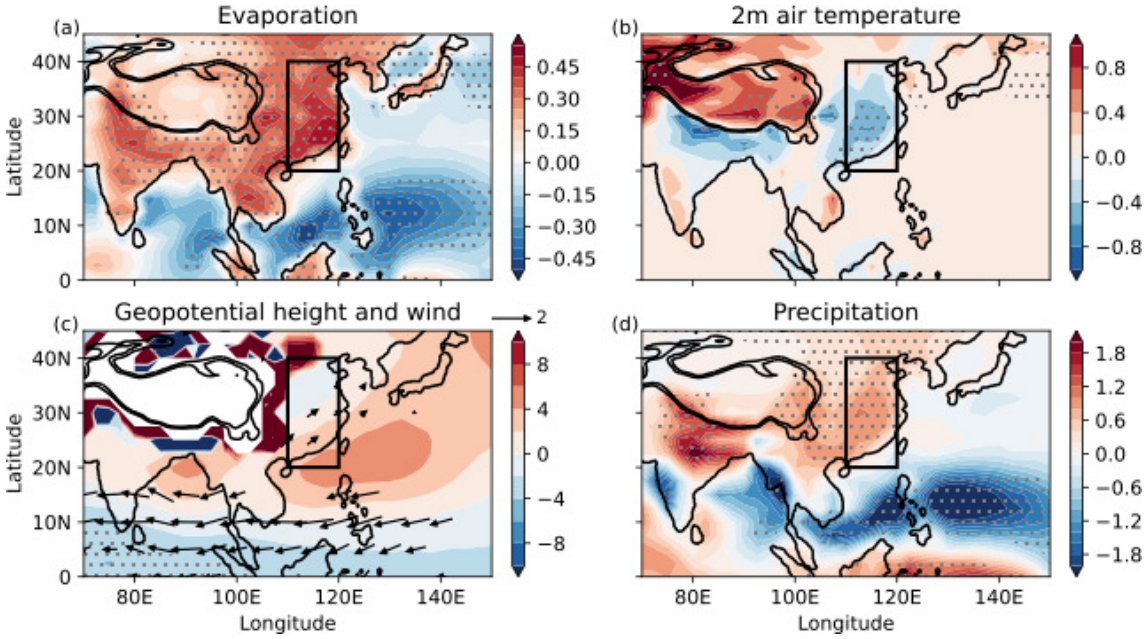

Fig. S8. As Fig. 3 in the main text, but excluding FGOALS-g3 and FGOALS-f3-L from the regression.

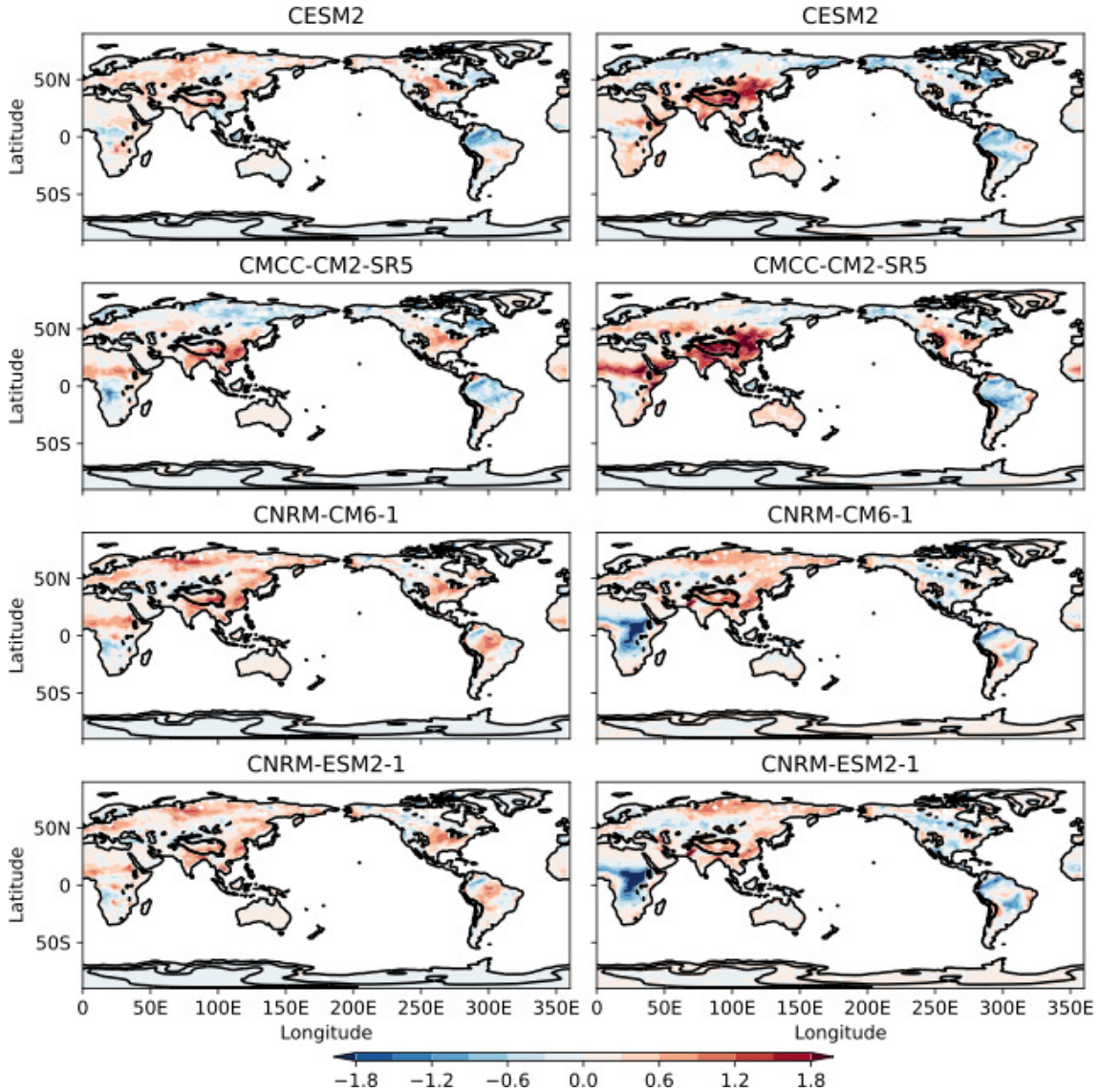

Fig. S9. Evapotranspiration bias (mm d^{-1}) relative to GLEAM for the *land-hist* (left column) and AMIP (right column) simulations from: CESM2, CMCC-CM2-SR5, CNRM-CM6-1 and CNRM-ESM2-1.

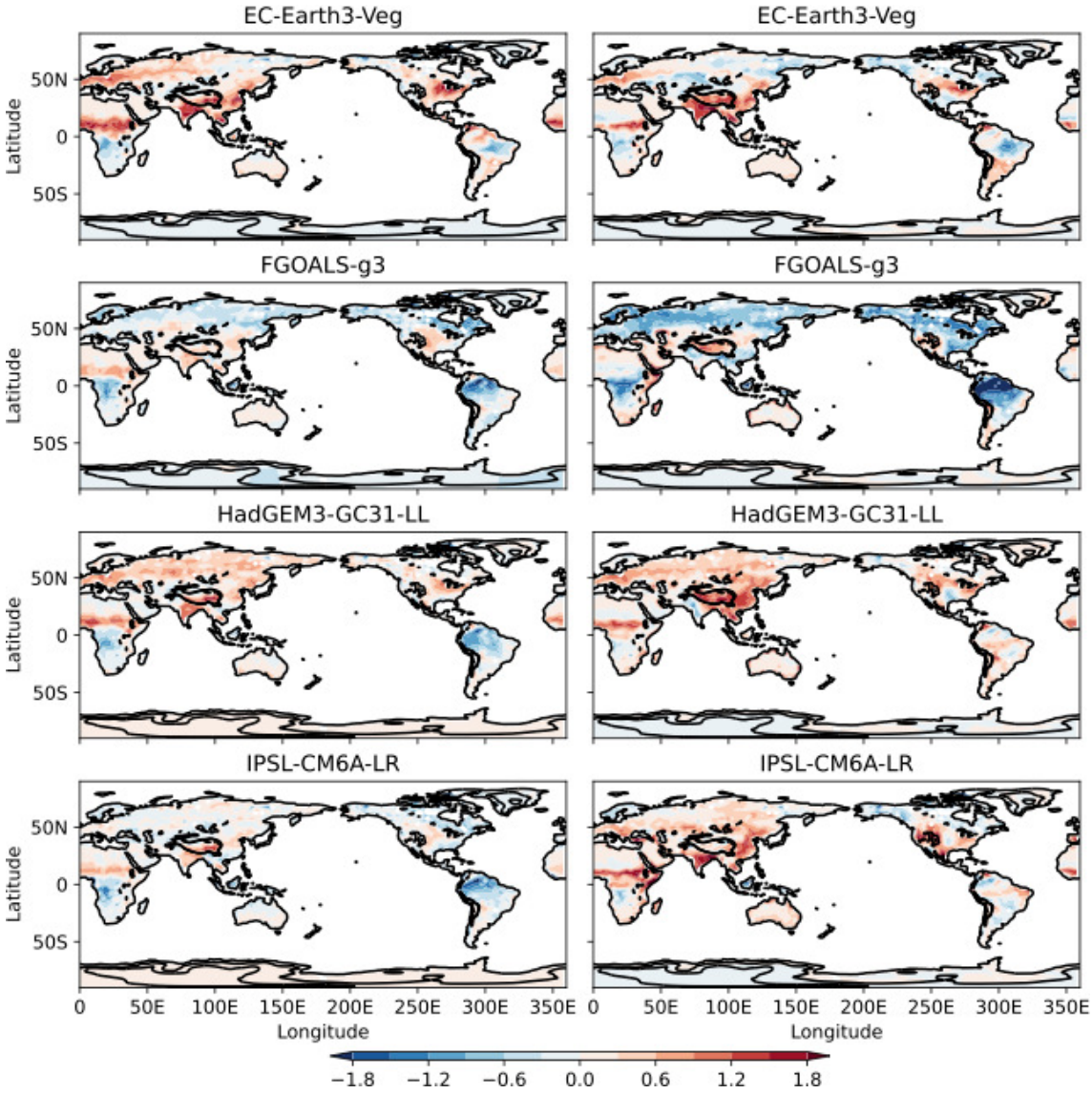

Fig. S10. As Fig. S9 but showing: EC-Earth3-Veg, FGOALS-g3, HadGEM3-GC31-LL and IPSL-CM6A-LR.

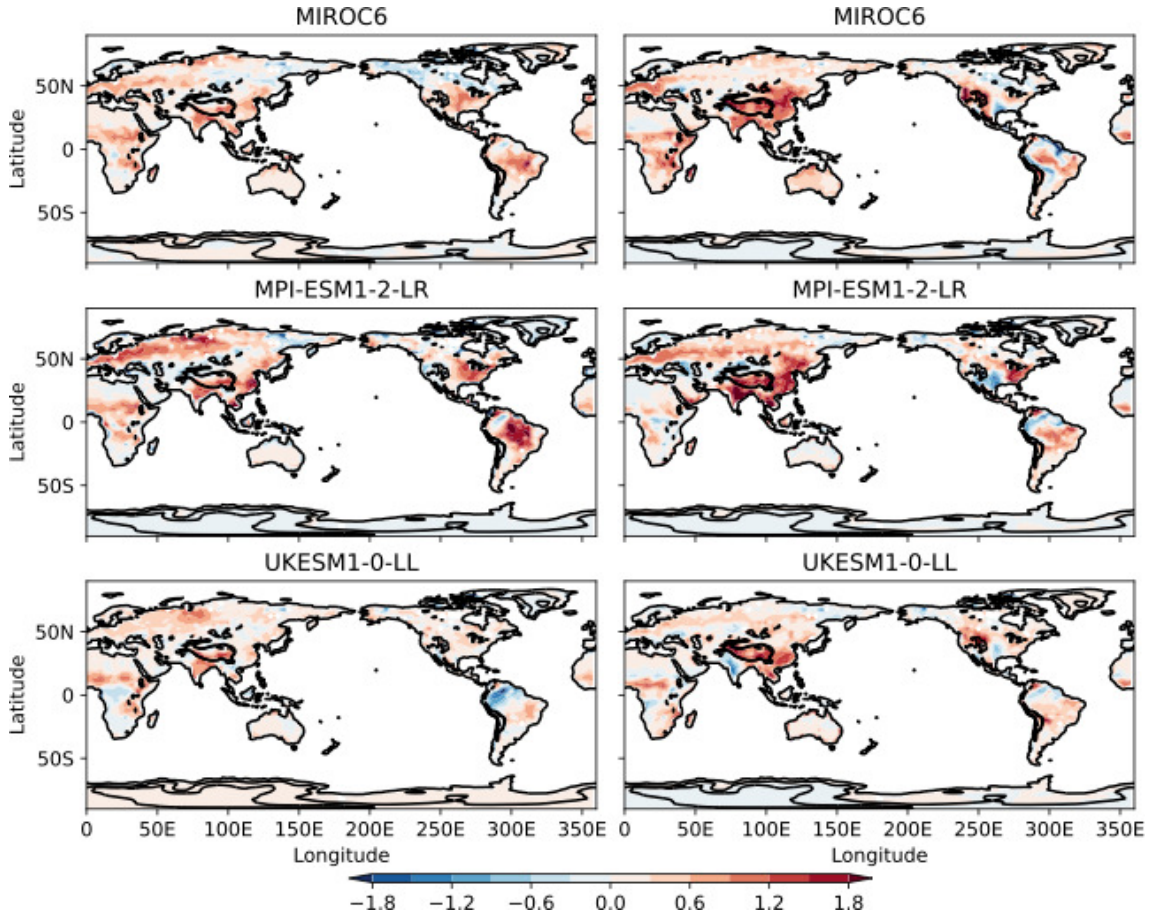

Fig. S11. As Fig. S9 but showing: MIROC6, MPI-ESM1-2-LR and UKESM1-0-LL.

REFERENCES

Beck, H. E., and Coauthors2019: MSWEP V2 Global 3-Hourly 0.1° Precipitation: Methodology and Quantitative Assessment. *Bull. Amer. Meteor. Soc.*, **100**(3), 473–500, http://doi.org/10.1175/BAMS-D-17-0138.1.

Frierson, D. M. W., Held, I. M., and Zurita-Gotor, P., 2006: A Gray-Radiation Aquaplanet Moist GCM. Part I: Static Stability and Eddy Scale. *J. Atmos. Sci.*, **63**(10), 2548–2566, https://doi.org/10.1175/JAS3753.1.

Manabe, S., 1969: Climate and the Ocean Circulation: 1. The atmospheric circulation and the hydrology of the Earth's surface. *Mon. Wea. Rev.*, **97**(11), 739–774, https://doi.org/10.1175/1520-0493(1969)097<0739:CATOC>2.3.CO;2.

Pietschnig, M., F. H. Lambert, M. Saint-Lu, andG. K. Vallis 2019: The Presence of Africa and Limited Soil Moisture Contribute to Future Drying of South America.*Geophys. Res. Lett.*, **46**(21), 12 445–12 453, https://doi.org/10.1029/2019GL084441.